Population analysis and immunologic landscape of melanoma in people living with HIV indicate impaired antitumor immunity

Lindsay N Barger[1,2,3], Derek Wang[4], Ashley L Saravia[3], Valeria Mezzano[5,6], Gyles Ward[6], Cynthia Loomis[5,6], Carly Feldman[7], Madalina Tuluc[8], Rino S Seedor[7,2], Peter J Gaskill[1,2], Anna E Coghill[9], Gita Suneja[10], Iman Dehzangi[4,11,12], Jennifer L Hope[3,2], George Jour[5,13], Gabriele Romano[1,2]*

[1]Department of Pharmacology and Physiology, Drexel University College of Medicine, Philadelphia, Pennsylvania.

[2]Immune Cell Regulation & Targeting Program, Sidney Kimmel Comprehensive Cancer Center, Philadelphia, Pennsylvania.

[3]Department of Microbiology and Immunology, Drexel University College of Medicine, Philadelphia, Pennsylvania.

[4]Center for Computational and Integrative Biology (CCIB), Rutgers University, Camden, New Jersey

[5]Department of Pathology, New York University Langone Medical Center, New York, New York

[6]Experimental Pathology, Division of Advanced Research Technologies, New York University Langone Medical Center, New York, New York.

[7]Department of Medical Oncology, Thomas Jefferson University Hospital, Philadelphia, Pennsylvania.

[8]Department of Pathology and Genomic Medicine, Jefferson University Hospital, Philadelphia, Pennsylvania.

[9]Cancer Epidemiology Program, Moffitt Cancer Center, Tampa, Florida

[10]Department of Radiation Oncology, Huntsman Cancer Institute, Salt Lake City, Utah

[11]Department of Computer Science, Rutgers University, Camden, New Jersey

[12]Rutgers Cancer Institute, Rutgers University, New Brunswick, New Jersey

[13]Department of Dermatology, New York University Langone Medical Center, New York, New York

***Correspondence:** Gabriele Romano – gr476@drexel.edu

Keywords: melanoma, HIV, T cells, MDSCs, immunotherapy, chronic infection

Funding: G.R. is supported by: WW Smith Charitable Trust - Medical Research Program (#C2303); Department of Defense - Congressionally Directed Medical Research Programs, Melanoma Research Program (ME220048); American Cancer Society (DBG-23-1036360-01); Comprehensive NeuroHIV Center (CNHC) Developmental Research and Mentoring Core (NIMH - P30MH092177); Sidney Kimmel Comprehensive Cancer Center (#00023568 and #901333). L.B. is supported by the Translational Research Training Grant in NeuroHIV (NIMH, T32-MH079785). P.J.G is supported by the National Institute of Drug Abuse, DA057337 and DA058051. Experimental Pathology Research Laboratory [RRID: SCR_017928] is partially supported by the Cancer Center Support Grant (P30CA016087). The original Akoya/PerkinElmer Vectra® multispectral imaging system was awarded through the Shared Instrumentation Grant S10 OD021747.

Acknowledgments: We thank the AIDS and Cancer Specimen Resource (ACSR) for providing tumor samples from PLWH; ACSR is funded by the National Cancer Institute.

Conflict of interest statement: The authors declare no conflicts of interest.

Abstract

Purpose: To dissect the clinical and immunological features of people living with HIV (PLWH) diagnosed with melanoma, who have consistently shown worse outcomes than HIV-negative individuals (PLw/oH) with the same cancer. **Experimental Design:** We analyzed electronic health records from 1,087 PLWH and 394,437 PLw/oH with melanoma. Demographic and clinical characteristics were compared. Spatial immune transcriptomics (72 immune-related genes) was performed on melanoma tumor samples (n=11), with downstream validation using multiplex immunofluorescence (n=15 PLWH, n=14 PLw/oH). **Results:** PLWH were diagnosed at a younger age, had greater representation of Hispanic and Black individuals, and showed reduced survival. They also had a markedly increased risk of brain metastases. PLWH experienced significant delays in initiating immune checkpoint inhibitor (ICI) therapy and had worse post-ICI survival, even after balancing covariates. Spatial transcriptomics revealed a more immunosuppressive tumor microenvironment in PLWH, with increased transcription of immune checkpoints (PD1, LAG3) and reduced antigen-presentation markers (HLA-DRB, B2M), with distinct spatial distributions in tumors and surrounding microenvironments. Multiplex immunofluorescence demonstrated features of an exhausted $CD8^+$ T cell compartment, including enrichment of $PD1^{int}LAG3^-$ and $PD1^{int}LAG3^+$ subpopulations, and a significant accumulation of myeloid-derived suppressor cells ($CD11b^+$ $HLA\text{-}DR^-$ $CD33^+$).

Conclusions: Melanoma in PLWH is associated with distinct clinical and immunological features, including delayed ICI treatment, reduced survival, and an immunosuppressive microenvironment with exhausted $CD8^+$ T cells and expanded myeloid-derived suppressor cells. These findings suggest that chronic HIV infection may impair antitumor immunity in melanoma. Targeting the pathways identified here may improve therapeutic responses and outcomes in this population.

Statement of translational relevance

This study reveals critical barriers to effective melanoma treatment in people living with HIV (PLWH). Despite receiving immune checkpoint inhibitors (ICIs), PLWH face delayed therapy initiation, a greater likelihood of brain metastases, and significantly higher long-term mortality, even after adjusting for demographic covariates. Transcriptional immune profiling further uncovers a tumor microenvironment enriched in immunosuppressive myeloid-derived suppressor cells and $CD8^+$ T cell populations with features of exhaustion. These findings suggest that poorer outcomes in PLWH stem not only from delayed care, but also from distinct targetable mechanisms of immune dysfunction. For example, strategies to reverse MDSC accumulation in the tumor or tailored ICI regimens could enhance immune responsiveness and improve treatment efficiency. By defining the clinical and immunological features of this population, this work highlights

opportunities for precision immunotherapy tailored to PLWH with melanoma, with direct implications for improving survival and reducing disparities.

Introduction

Advancements in antiretroviral therapies (ART) have transformed HIV infection from a terminal diagnosis into a chronic condition, allowing people living with HIV (PLWH) to achieve a life expectancy nearly equal to that of the general population [1,2]. However, despite the success of ART in suppressing viral replication, HIV remains a lifelong infection due to its ability to integrate into host genomes and establish a state of latency, particularly within long-lived memory T cells and myeloid cells in sanctuary sites [3-5]. While ART prevents the spread of the infection, it does not eliminate pre-existing reservoirs that harbor integrated and latent viruses, leaving PLWH with persistent immune dysregulation and, therefore, increased susceptibility to age-related diseases [6]. Among these, non-AIDS-defining cancers (NADCs) have emerged as a major cause of mortality, including cutaneous melanoma [6]. Several reports on melanoma in PLWH point to disproportionately worse clinical outcomes compared to melanoma patients without HIV, despite adjustment for key factors such as disease stage at presentation [7-9]. The mechanisms underlying this disparity remain poorly understood. It is largely unknown how chronic HIV infection alters anti-tumor immune responses, which is particularly relevant in melanoma, where immune regulation is central to disease progression and treatment response.

To address this major knowledge gap, we first analyzed publicly available clinical datasets to compare demographics and outcomes between PLWH and people living without HIV (PLw/oH), revealing significant disparities in demographics, metastasis risk, and survival after a melanoma diagnosis. We then performed the first immune-focused spatial transcriptomic analysis of melanoma tumors according to patient HIV status, uncovering striking differences in tumor-associated T cell and myeloid populations in PLWH. These findings were further validated and expanded using multiplex immunofluorescence to characterize immune cell phenotypes and subpopulations. Together, our data reveal a profoundly altered immune landscape in melanoma among PLWH, marked by T cell exhaustion and myeloid-mediated suppression, which underscores the need for tailored therapeutic strategies in this population with suboptimal clinical outcomes.

Methods

Clinical electronic record patient dataset

The data used in this study were collected on 10/08/2025 from the TriNetX Research Network, which provided access to electronic medical records (diagnoses, procedures, medications) from approximately 157,574,584 patients from 111 healthcare organizations. Patient demographics include date of birth, age, sex, marital status, race, and ethnicity. Demographics are coded to HL7 version 3 administrative standards. For the survival studies, the date a patient was reported as “Deceased” in the dataset was used; the cause of death was not available in the dataset. The “Deceased” term in the TriNetX data model pools together several different sources of mortality data: documented mortality by HCOs using ICD-10 code R99 (ill-defined

and unknown cause of mortality); if mortality is reported from HCOs via death dates of patients, this is also captured and mapped to the “Deceased” term; for the subset of patients on the TriNetX networks that have additional mortality data linked to their electronic health records (closed claims, social security master death file, private obituaries, etc.), these additional sources are also mapped to the “Deceased” term. Diagnoses and medication data in the TriNetX database are obtained from electronic health records of participating healthcare organizations. Diagnoses are recorded using the ICD-10 standardized coding system, while medication information is captured through prescription and dispensing records. These data may originate from clinical documentation, problem lists, billing records, or insurance claims and are harmonized across sites to ensure consistency.

Two cohorts of patients were retrieved with the following criteria: PLWH cohort was built selecting patients that had Malignant melanoma of skin (ICD code C43) and Human immunodeficiency virus [HIV] disease (ICD code B20, 1,087 patients were retrieved); PLw/oH cohort was built selecting patients that had C43 but not code B20 (394,437 patients were retrieved). Only patients with a cancer diagnosis between 2005 and 2025 were included. Only patients with a cancer diagnosis after HIV were included in the PLWH cohort.

The following ICD codes were used for metastatic disease: C78.7 (liver and bile duct), C79.3 (brain and meninges), C77 (lymph nodes), and C78.0 (lung). Two different analyses were performed for patients with an early occurrence of metastatic disease (from day 1 to 6 months after diagnosis) and patients with a later occurrence of metastasis (6 months from melanoma diagnosis onwards). For the “All sites” category, patients who had any of the metastatic codes C77, C78.0, C79.3, and C78.7 were included. For co-morbidity assessment, the following codes were used: I20-I25 (Ischemic heart diseases), I11 (Hypertensive heart disease), J40-J4A (Chronic lower respiratory diseases), N18 (Chronic kidney disease CKD), B18 (Chronic viral hepatitis), and E10 (Type 1 diabetes mellitus). In the dataset, medications are represented at the level of ingredients, coded to RxNorm, and organized by VA or ATC classification. For the analysis of immunotherapy characteristics and outcomes, the two cohorts were filtered to include only patients who had received any of the following FDA-approved immune checkpoint inhibitors: 1094833 (ipilimumab), 1597876 (nivolumab),1547545 (pembrolizumab), 1792776 (atezolizumab), 1919503 (durvalumab), or 2596773 (relatlimab).

Inclusion and Ethics

These studies were conducted in accordance with recognized ethical standards, including the U.S. Common Rule and the Declaration of Helsinki. The retrospective study was exempt from informed consent and Western Institutional Review Board (IRB) review. All data analyzed were part of a secondary analysis of existing records, involved no intervention or interaction with human subjects, and were fully de-identified in accordance with the de-identification standard outlined in Section §164.514(a) of the HIPAA Privacy Rule. De-identification was performed and formally certified by a qualified expert, as defined in Section §164.514(b)(1), with the determination most recently renewed in December 2020.

Spatial Immune Transcriptomics

De-identified melanoma patient samples were acquired from the AIDS and Cancer Specimen Resource, the Sidney Kimmel Comprehensive Cancer Center, and NYU Grossman School of Medicine. Sample collection and handling were evaluated by institutional IRB. 11 melanoma samples from people living with HIV were retrieved first, and 11 HIV-uninfected controls were then selected to match age, sex, race, and ethnicity, and nature of specimens (**Table S1**). Five-micron sections were prepared after cleaning the microtome and recovering sections in RNAse-free water. Slides were processed per NanoString® protocols for nCounter RNA GeoMx experiments. Slides were baked at 60°C for 2 hours and loaded onto a BOND Rx stainer (Leica). Antigen retrieval was performed with EDTA-based solution (pH 9, ER2 Leica, AR9640) at 100°C for 20 minutes, followed by proteinase K (Ambion, AM2546) treatment (1 µg/mL, 15 minutes, room temp). Slides were stored in PBS and incubated overnight with 200 µL of GeoMx Immune Pathways Hs RNA Probes (121300201) at 37°C in a HybEZ™ oven under a Hybrislip. Post-hybridization, slides underwent two washes in 50% Formamide-4XSSC at 37°C and two washes in 2XSSC at room temperature, then labeled with RNA-compatible melanoma morphology markers (GeoMx Melanoma Morph Kit Hs RNA). All slides were processed together but loaded onto the GeoMx instrument in batches of four. Automated fluorescence imaging at 20X magnification (0.4 µm/px) was followed by ROI selection. For each sample, three to five regions of interest (ROIs) were selected for analysis. ROI selection and masking were performed in collaboration with a board-certified dermatopathologist to ensure accurate discrimination between tumor and tumor-microenvironment compartments. ROIs were identified based on morphological assessment and multiplex immunofluorescence staining for S100B/Pmel17 (melanocytic markers), CD45 (pan-leukocyte marker), and DAPI (nuclear counterstain). Tumor-cell–rich (TUMOR) regions were defined as areas enriched in melanoma cells, characterized by cohesive nests of S100B/Pmel17^{+} cells with consistent nuclear morphology and limited CD45^{+} immune infiltration. Tumor-microenvironment–rich (TME) regions were defined as areas negative for melanocytic markers (S100B/Pmel17^{-}) and enriched in CD45^{+} immune cells and/or stromal components, representing the surrounding immune and stromal microenvironment. Following ROI identification, digital masks were applied to precisely capture TUMOR (green) and TME (red) subregions (**Fig. S1**). ROIs were UV-illuminated (~1 µm² resolution) to release barcodes, which were aspirated and transferred to a 96-well plate. Eluted material was stored at -20°C until processing at NYUGSM. Plates were lyophilized at 65°C for 1–2 hours, rehydrated in DEPC water, mixed with ICP-hyb buffer and GeoMx Hyb Code Pack_RNA probes (121300402), and incubated overnight at 65°C. Hybridized samples were pooled by column and run on the nCounter MAX/Flex system to generate RCC files, which were analyzed using the GeoMx Control Center.

Read counts were normalized to the geometric mean of five housekeeping genes (OAZ1, POLR2A, RAB7A, SDHA, UBB). Normalized read counts are reported in **Table S2**. Differential expression analysis

180 (DEGs) was conducted on the normalized read counts using the DEseq2 algorithm [10] in R v4.4.2 to compare
181 the TME and TUMOR across HIV-positive and HIV-negative patients.
182
183 *Immune pathways and population analysis*
184 The MCP-counter algorithm was used to calculate the enrichment scores of tailored gene sets[11]. We
185 conducted two marker gene–based analyses: one focusing on differences in immune signaling gene
186 expression (53 genes, **Table S3**), and another on estimating immune cell population abundances (19 genes,
187 **Table S4**). A multiple Welch t-test was then performed on the population or pathway scores in HIV+ vs. HIV-
188 samples. Data were represented in a bubble plot with the adjusted p-value (q-value) and Log2 fold change
189 (HIV+ vs. HIV-) for the TUMOR and TME areas (R v4.4.2; ggplot2 package).
190
191 *Multiplex Immunofluorescence (mIF)*
192 mIF staining was performed on 5 µm paraffin sections with Akoya Biosciences® Opal™ reagents on
193 a Leica BondRx autostainer, according to the manufacturer's instructions. In brief, sections were treated with
194 hydrogen peroxide to block endogenous peroxidases, followed by antigen retrieval using ER2 (Leica
195 AR9640) at 100°C. Primary and secondary antibodies were applied sequentially, with each pair followed by
196 HRP-mediated tyramide signal amplification using a unique Opal® fluorophore. After each staining round,
197 antibodies were stripped via heat retrieval, leaving the fluorophore covalently bound at the antigen site.
198 Sections were counterstained with spectral DAPI (Akoya FP1490) and mounted with ProLong Gold Antifade
199 (ThermoFisher P36935). Imaging was performed using a Leica AT2 (40X) or Akoya Vectra Polaris (20X), and
200 qptiff scans were generated with PhenoImagerHT 2.0, Phenochart 2.0, and InForm 3.0. Scans were analyzed
201 in QuPath with four ROIs per sample—two central and two peripheral—independently selected by two
202 operators using fixed-threshold detection. Averages of ROIs and operators were used as replicates. Total
203 cells were detected via QuPath's DAPI-based algorithm. T cell and myeloid infiltrates were assessed using
204 two antibody panels: Panel 1 (CD8, CD4, FoxP3, Lag3, PD1, **Table S5**) and Panel 2 (CD11b, CD33, HLA-
205 DR, CD66b, **Table S6**).
206 A custom QuPath script was developed to classify CD8+ T cells and respective PD1 expression into
207 three tiers (low, intermediate, and high), with an additional subdivision for LAG3 positivity. PD1 intensity
208 thresholds were manually defined after visual review by two independent operators to capture biologically
209 distinct expression levels. Based on this consensus, cells with PD1 intensity between 0.0 and 0.2 were
210 classified as PD1 negative, while those with intensities above 3.0 were designated as PD1 high. The
211 intermediate tier (0.2–3.0) captured cells with PD1 expression levels falling between these two extremes. A
212 similar script was generated for CD4+ T cells and relevant subpopulations. CD11b+ myeloid cells and their
213 co-expression with HLA-DR, CD33, or CD66b were quantified similarly.
214
215 *Statistical analysis*

Data was checked for normality (Kolmogorov-Smirnov, Shapiro-Wilk test) prior to being assigned to parametric or non-parametric analyses. All the datasets analyzed in this work displayed a normal distribution. To compare significant differences between two groups, we used a two-tailed t-test (parametric; Welch correction was applied if variances were different between groups). A $p<0.05$ was considered significant. For demographic and clinical covariates, univariate T-test analysis was performed. For the immune pathways and population analysis, a multiple Welch t-test was performed with an FDR of 0.01. An adjusted p-value (q-value)<0.01 was considered significant. For survival studies, a Log-rank (Mantel-Cox) test was used to detect differences in survival between two populations. A $p<0.05$ was considered significant. Hazard ratios (HRs) with 95% confidence intervals (CIs) were calculated using Cox proportional hazards regression. The HR compares the hazard rates—the instantaneous rate at which patients experience the outcome for the first time—between two cohorts. An HR of 1 indicates equal rates of the outcome at any point in time, whereas an HR >1 (or <1) indicates that one cohort experiences the event at a higher (or lower) rate than the other. HR estimates are reported with 95% CIs, and if the CI includes the null value of 1, the difference is not considered statistically significant. The proportional hazards assumption was assessed via the Grambsch–Therneau test based on scaled Schoenfeld residuals, which evaluates whether covariate effects vary over time (a $p<0.05$ indicates a non-proportional hazard). For risk Ratio assessment, risk ratios with 95% confidence intervals are calculated to compare outcomes between cohorts. Risk was defined as the percentage of patients in the cohort who had the outcome in the time window (Risk = Patients with Outcome/Patients in Cohort). Risk Ratio was defined as the ratio of risk between cohorts (Risk Ratio = Risk for Cohort 1 / Risk for Cohort 2). Cohort balancing in TriNetX was conducted using propensity score–based methods. Propensity scores were estimated via logistic regression models incorporating baseline demographic and clinical covariates. Patients were matched 1:1 using greedy nearest-neighbor matching without replacement, applying a caliper of 0.1 pooled standard deviations of the logit of the propensity score to minimize residual confounding. In addition to matching, inverse probability of treatment weighting (IPTW) was applied as a sensitivity approach, assigning weights based on the inverse of the estimated propensity score to create a pseudo-population in which covariate distributions were independent of exposure status. Balance across matched or weighted cohorts was evaluated by comparing standardized mean differences (SMDs) for each covariate, with thresholds of <0.1 considered evidence of acceptable balance. TriNetX Live was utilized to perform all the population analyses. To ensure patient confidentiality, TriNetX applies an automated privacy protection rule that rounds or suppresses cell counts ≤10. This masking affects only the display of data and does not influence statistical analyses, cohort matching, or aggregate calculations, which are performed using the complete, unmasked dataset. GraphPad Prism v.10.4.1 was utilized to perform all the other statistical tests.

Data Availability

Raw patient-level data from the TriNetX dataset cannot be publicly shared due to data use agreements and privacy protections. Interested investigators may reproduce our analyses or request access to limited datasets through TriNetX under institutional data-use agreements and IRB approval by contacting TriNetX directly (join@trinetx.com). All analyses were conducted using the platform's graphical cohort builder and built-in analytics tools; no custom code was used. The complete results of the GeoMX spatial transcriptomics experiment, including ROI-level metadata and normalized expression values, are provided in **Table S2**. mIF raw images are available upon request.

Results

PLWH with melanoma display increased overall mortality rates and brain metastasis risk.

To evaluate population differences between people living with and without HIV (PLWH and PLw/oH) diagnosed with melanoma, we interrogated the publicly available TriNetX Research Network dataset. Our study included two cohorts: 1,087 PLWH with melanoma and 394,437 melanoma patients without HIV. Univariate analysis of baseline demographics revealed that PLWH were diagnosed with melanoma at a younger age (58.6 ± 12.2 years in PLWH vs. 62.8 ± 15.6 years in PLw/oH) and were more likely to be male (81% vs. 52%, **Table 1**). Racial and ethnic distribution also differed between the total cohorts. PLWH with melanoma exhibited a higher representation of Hispanic or Latino individuals (4% vs. 2%) and Black or African American individuals (7% vs. 1%) compared to their non-HIV counterparts (**Table 1**).

PLWH experienced a worsened long-term prognosis with a significantly lower ten-year survival rate (73.04% vs 77.95%, PLWH vs. PLw/oH, p=0.00628, **Fig. 1A**, **Table S7**), also seen in previous reports [7]. The two cohorts had a similar median follow-up time of approximately 3.4 years (PLw/oH) and 4.2 years (PLWH, **Table S8**). Our analysis focused on patients diagnosed during the ART era (98.4% of patients had ART treatment records; patients diagnosed before 2005 were not available). Staging information and BRAF status were only available for <1% of the population, and no robust statistical assessment could be performed on these aspects. Nevertheless, given the impact of metastasis on cancer mortality, we assessed the occurrence of melanoma spreading to its most frequent metastatic sites. At presentation, the PLWH cohort displayed significantly increased occurrence of metastasis for all the analyzed sites (**Table 1**). We then assessed the risk of metastasis occurring after melanoma diagnosis. No significant differences were detected between the two groups of patients in terms of early metastasis (1 day to 6 months after diagnosis, **Table S9**). While there were no significant differences in lung, liver, or lymph node metastases, PLWH had a significantly higher risk of late brain metastases (>6 months after diagnosis, p=0.0009, risk ratio = 1.78, **Table S9**), and an overall increased risk of metastatic disease in the long term (p=0.0296, risk ratio = 1.325, **Table S9**). PLWH have also been reported to experience higher rates of chronic conditions affecting the heart, lungs, and liver, as well as diabetes, a trend that we observed in our cohort as well (**Table 1**). To account for potential confounders, including metastasis, other common chronic conditions, and demographic factors, we

286 balanced the cohorts for these covariates (**Table 1**) and found significantly different survival rates even after
287 adjustment (73.37% vs 81.16% survival rate, PLWH vs. PLw/oH, p=0.02411, **Fig. 1B, Table S10**).
288 Next, we focused on FDA-approved immune checkpoint inhibitors (ICIs) to evaluate differences in
289 treatment patterns and outcomes between the two groups. ICIs serve as the first-line treatment approach for
290 patients with advanced melanoma, and analyzing their use provides insights into how patients with late-stage
291 disease fare in the clinical setting. Among our cohorts, approximately 9% of PLWH (n=95) and 6% of PLw/oH
292 (n=23,827) had a record of receiving immune checkpoint therapies. The demographic features of these two
293 sub-groups reflected most of the differences we detected between the parent cohorts (**Table 2**). Although
294 we were not statistically powered enough to draw conclusions for specific treatment regimens, we were able
295 to make some comprehensive observations regarding ICI outcomes and timing. We found that, on average,
296 PLWH experienced longer delays before initiating treatment compared to PLw/oH (p=0.0026, **Tables S11-**
297 **12**). In the PLWH cohort, we did observe a significantly higher number of patients with lymph node metastasis
298 at presentation (**Table 2**). Once ICI was initiated, we did not detect differences in treatment duration (**Table**
299 **S12**). We then performed a ten-year survival analysis of the two cohorts. PLWH demonstrated significantly
300 lower probabilities of survival compared to the non-HIV melanoma patients (10-year, 27.14% vs 46.91%
301 survival rate, PLWH vs. PLw/oH, p=0.04696, **Fig. 1C**, and **Table S13**). Such significant differences persisted
302 even after adjusting for demographic covariates, metastasis at presentation, and major co-morbidities (10-
303 year, 29.92% vs 69.54% survival rate, PLWH vs. PLw/oH, p=0.03129, **Fig. 1D**, **Table 1, and Table S14)**
304
305 **PLWH display an immunosuppressive and exhausted melanoma tumor microenvironment**
306 Our data indicate that PLWH who develop melanoma experience an overall elevated mortality rate,
307 also in the sub-cohort who received ICI. While demographic differences, higher rates of coexisting conditions,
308 and psychosocial barriers are contributors to mortality, the decreased survival rate persisted even after
309 balancing cohorts for demographic and clinical covariates, indicating there may also be underlying biological
310 or immunological components. To explore this, we collected tumor samples from 11 PLWH with melanoma
311 and matched them with samples from 11 PLw/oH with melanoma with similar clinical and demographic
312 features (**Table S1)**.
313 For each sample, three to five regions of interest (ROIs) were selected for spatial immune
314 transcriptomic profiling (72 immune-related genes). A dermatopathologist defined ROIs based on
315 morphological features and immunofluorescence staining for melanocytic markers, designating subregions
316 as either tumor-cell–rich (TUMOR) or tumor-microenvironment-rich (TME) (**Fig. S1**). TUMOR ROIs
317 corresponded to areas enriched in melanoma cells (positive for S100B/Pmel17) with limited immune
318 infiltration, whereas TME ROIs encompassed $CD45^+$ immune- and stroma-rich regions lacking tumor marker
319 expression. This classification was designed to capture both tumor-invasive immune niches and the
320 surrounding immune microenvironment. To identify transcriptional differences related to HIV status, we
321 performed differential expression analysis (DEGs) using the DESeq2 algorithm, comparing both TME and

322 TUMOR regions between PLWH and PLw/oH. The analysis revealed significant gene expression differences
323 between the groups, highlighting distinct immune signatures and checkpoint expression patterns associated
324 with HIV status (**Fig. 2**).

325 When comparing the TME and TUMOR areas of PLWH with PLw/oH, we observed increased
326 expression of several immune checkpoint genes, including *PD1*, *LAG3*, *CTLA4*, *TIGIT*, *CD276,* and *ICOSLG*.
327 Notably, *LAG3* emerged as the top-scoring immune checkpoint in the TUMOR, while *PD1* was the highest in
328 the TME (**Fig. 2A- B**). This suggests that there are distinct spatial distributions of varying T cell populations
329 within these tumors. Both the TUMOR and TME exhibited additional characteristics of an immune-
330 suppressive or evasive microenvironment. In the TUMOR compartment, we observed elevated expression
331 of *IDO1*, a key protein that inhibits T-cell function (**Fig. 2A**). Meanwhile, the TME showed reduced expression
332 of *HLA-DRB* and *B2M,* which are MHC class II and I molecules essential for antigen presentation (**Fig. 2B**).
333 Several key genes involved in immune responses were also downregulated, including *IFNGR1*, *CD74*, *LY6E*,
334 and *STAT2*. Beyond immune regulation, we identified a pattern of differential gene expression pertaining to
335 fibrosis and extracellular matrix (ECM) remodeling in the TME. PLWH demonstrated a decline in the
336 expression of *CD44*, *ITGAV*, *and PECAM1* and increased *ITGB8*, suggesting alterations in tumor-stroma
337 interactions that may contribute to disease progression (**Fig. 2B**).

338 Additionally, a small cadre of genes associated with enhanced inflammation was identified in the TME
339 of PLWH, including an increase in *IL-15*, *TBX21*, and *CCL5* (**Fig. 2B**). In the TUMOR, there was an increase
340 in *BATF3*, which is mostly expressed on $CD8^+$ cells (i.e., dendritic cells and T cells) (**Fig. 2A**).

341 To summarize our findings and prioritize downstream validation, we ran a modified version of the
342 MCPcounter algorithm, utilizing tailored gene sets that included population marker genes and immune
343 signaling genes (**Tables S3-S4**). The only two upregulated gene sets in PLWH, both in TME and TUMOR
344 areas, were immune checkpoints and myeloid suppressive signaling (**Fig. 2C**). In terms of immune
345 populations, overall, it appeared that the TUMOR areas from PLWH were generally enriched in immune cells
346 both from myeloid and lymphoid origin and displayed enhanced expression of several immune signaling
347 pathways (**Fig. 2C and Fig. S2**). The TME areas were, in general, more similar between PLWH and PLw/oH
348 (**Fig. S2**).

349

350 **PLWH display distinct subsets of $CD8^+$ T cells within the melanoma tumor environment**

351 To validate and further expand upon the spatial transcriptomics findings, we investigated T cell
352 populations using multiplexed immunofluorescence staining (mIF). The cohort included melanoma tumor
353 samples from 15 HIV^+ and 14 HIV^- patient samples, with 11 samples in each group overlapping with those
354 profiled by spatial transcriptomics (**Fig. S3** and **Table S1**). We examined T cell populations within both the
355 tumor bulk and peripheral edges using an mIF panel targeting T cell populations (CD8, CD4, Foxp3), along
356 with the two top-scoring immune checkpoint inhibitors identified in our transcriptional analysis (LAG3 and
357 PD1) (**Fig 3A**). While melanocytic markers were excluded from this panel, a pathologist histologically

358 assessed the sections to delineate tumor regions and guided the analysis. Thus, the results reflect the tumor
359 specimens as a whole instead of the specific delineation of sub-regions.

360 Analysis of the T cell compartment revealed no significant differences in the overall frequency of $CD8^+$
361 or $CD4^+$ T cells between melanoma tumors in PLWH and uninfected patients (**Fig. 3B-C**). Similarly, regulatory
362 T cells (T_{REG}, $CD4^+FOXP3^+$) abundance did not differ significantly between groups (**Fig. S4A**). Notably, PLWH
363 exhibited altered T cell proportions, with a significantly reduced $CD4^+$:$CD8^+$ ratio and a lower $Foxp3^+$:$CD8^+$
364 ratio, suggesting a shift in the relative balance of T cell subsets (**Fig. 3D-E**).

365 We next interrogated the co-expression of immune checkpoint receptors PD1 and LAG3 on $CD4^+$
366 and $CD8^+$ T cells. PD1 expression was stratified into three tiers ($PD1^-$, $PD1^{int}$, and $PD1^{high}$), and LAG3 into
367 two ($LAG3^-$ and $LAG3^+$), based on previous reports highlighting functional differences in cytotoxicity and
368 exhaustion in these subpopulations[12-14]. No significant differences were observed in $CD4^+$ T cell subsets
369 between PLWH and PLw/oH (**Fig. S4B-E**).

370 Notably, we identified distinct subpopulations of $CD8^+$ T cells in PLWH compared with PLw/oH.
371 Specifically, melanoma tumors from PLWH showed significant enrichment of the $CD8^+PD1^{int}LAG3^-$ and the
372 $CD8^+PD1^{int}LAG3^+$ populations (**Fig. 3F-G**). Notably, we did not detect any differences in the abundance of
373 $PD1^{HIGH}$ cells, whether they were $LAG3^+$ or $LAG3^-$ (**Fig. 3H-J**).
374

375 **PLWH exhibit an enriched population of immunosuppressive myeloid cells in melanoma**
376 **tumors**

377 Given the important role of the myeloid compartment in modulating T cell function, we next turned our
378 focus to tumor-associated myeloid populations. Pathway analysis highlighted myeloid suppressive signaling
379 as a top candidate (**Fig. 2C**) and a significant downregulation of key components of antigen presentation,
380 such as *HLA-DRB*, within the tumor regions (**Fig. 2**). In parallel, previous studies have reported that PLWH
381 have elevated levels of myeloid-derived suppressor cells (MDSCs) at baseline, a population of highly
382 immunosuppressive, immature myeloid cells [15,16]. Based on these findings, we selected CD11b to broadly
383 define the myeloid lineage and included HLA-DR, CD33, and CD66b to resolve subpopulations (**Fig. 4A**),
384 including potential MDSCs. Using multiplexed immunofluorescence (mIF) on the tumor samples previously
385 analyzed for T cell populations, we identified a significant increase in $CD11b^+$ $HLA\text{-}DR^-$ myeloid cells in
386 PLWH (**Fig. 4B**), indicating an immature or non-antigen-presenting phenotype. Most of these cells also
387 expressed CD33, supporting their classification as monocytic-like MDSCs (M-MDSCs) (**Fig. 4C**). In contrast,
388 no differences were observed in $CD11b^+$ $HLA\text{-}DR^-$ $CD66b^+$ cells, or polymorphonuclear-like MDSCs (PMN-
389 MDSC) between PLWH and PLw/oH (**Fig. 4D**) [17].
390

391 Discussion

392 The present study demonstrates that PLWH who develop melanoma experience distinct clinical
393 outcomes and tumor microenvironments compared to those without HIV. Notably, PLWH exhibited increased

394 overall mortality, including in the subpopulation of patients who underwent ICI, even after adjusting for
395 demographic and clinical covariates. Immune-focused spatial transcriptomics analysis revealed a more
396 suppressive and likely exhausted tumor microenvironment (TME) in PLWH, which was further supported by
397 multiplex immunofluorescence identifying unique $CD8^+$ T cell subsets and an increased presence of myeloid
398 derived suppressor cells (MDSCs).

399 Despite increasing evidence of ICI safety in PLWH[18], this patient population has been largely
400 excluded from oncology clinical trials, resulting in limited efficacy data and persistent provider hesitancy [19,20].
401 This exclusion reflects broader patterns of delayed cancer treatment in PLWH, potentially driven by
402 disparities in healthcare access, treatment prioritization, and clinical decision-making. Our findings echo
403 these systemic gaps, demonstrating that PLWH experience significant delays in treatment initiation, likely
404 driven by both clinical uncertainty and psychosocial barriers, including limited access to care and persistent
405 medical mistrust rooted in historical HIV-related stigma, as we have previously reviewed [21]. Addressing these
406 barriers is critical to improving melanoma outcomes and ensuring equitable cancer care for PLWH.

407 We also found a significantly higher long-term risk of metastasis in PLWH, particularly to the brain.
408 As HIV infection is well known to develop into HIV-associated neurocognitive disorder (HAND)[22], this may
409 reflect an HIV-related disruption of the blood-brain barrier, creating a permissive environment for melanoma
410 colonization[23]. Given that brain metastasis significantly lowers survival and treatment responses, this
411 highlights the importance of heightened cancer surveillance and early treatment strategies for this population
412 [24,25].

413 In the ICI-treated cohort, none of whom received prior targeted therapy - an established factor for ICI
414 responsiveness - PLWH displayed decreased survival despite similar time on treatment. These data raise
415 the possibility that ICI may not confer the same durable responses in PLWH, which warrants further
416 investigation[26].

417 In addition to the clinical characteristics of melanoma in PLWH, our study provides critical insights
418 into how chronic HIV infection fundamentally alters the tumor immune landscape, potentially driving
419 worsened outcomes for this population of patients. We identified two enriched $CD8^+$ T cell subsets: $CD8^+$
420 $PD1^{INT}$ $LAG3^+$ and $CD8^+$ $PD1^{INT}$ $LAG3^-$. These subsets likely represent recently activated or pre-exhausted
421 phenotypes, with LAG3 co-expression acting as a stronger predictor of exhaustion.

422 PD1 and LAG3 are inhibitory receptors upregulated on $CD8^+$ T cells during chronic viral infections
423 and within tumors. While initially markers of activation, sustained co-expression drives T cell exhaustion.
424 Similar levels of $CD8^+$ $PD1^{HIGH}$ T cells observed in both PLWH and PLw/oH likely reflect chronic stimulation
425 by tumor antigens or PD-L1 expression [27-29]. However, PLWH showed increased $CD8^+$ $PD1^{INT}$ $LAG3^{+/-}$ T
426 cells, suggesting a population of recently activated or pre-exhausted T cells. LAG3 co-expression indicates
427 progression towards exhaustion, with their fate influenced by tumor-derived cues. Supporting this
428 interpretation, spatial transcriptomic analysis revealed elevated *LAG3* transcription localized near tumor
429 cells, consistent with a spatially driven gradient of exhaustion. PD1 and LAG3 co-expression on $CD8^+$ T cells

has been linked to impaired anti-tumor immunity, and while dual blockade of PD1 and LAG3 has shown promise in improving progression-free survival in metastatic melanoma [30-32], clinical data on ICI efficacy in PLWH remain scarce, particularly for anti-LAG3 therapies. Further research is needed to define how these pathways shape tumor progression in PLWH and inform targeted therapies to restore immune function.

Despite HIV's well-documented impact on the $CD4^+$ T cell compartment [33,34], we observed no significant differences in total $CD4^+$ T cell counts or their subsets between cohorts, suggesting that immune dysregulation in the TME of PLWH is primarily driven by $CD8^+$ T cells. This is further supported by a decreased CD4:CD8 ratio in PLWH.

Transcriptomic and multiplex IF analyses pointed to a shift in the myeloid compartment: a downregulation of antigen presentation genes and a shift from classical to cross-presentation mechanisms, indicative of an immune-evasive or immunosuppressive myeloid phenotype [35-37], supported by an accumulation of $CD11b^+$ $HLA\text{-}DR^-$ $CD33^+$ cells in melanoma tumors of PLWH. These cells, defined as myeloid-derived suppressor cells (MDSCs), are a rare and potent immunosuppressive subset of immature myeloid cells. In healthy individuals, MDSCs typically emerge later in cancer progression and are known contributors to immune evasion and resistance to immunotherapy [38,39]. However, PLWH exhibit elevated baseline levels of circulating MDSCs, regardless of ART status, likely due to chronic low-level inflammation[15,17]. This may promote early recruitment of MDSCs to the melanoma TME, accelerating melanoma progression in this population by impairing the T cell response [15-17,40-42]. Our data support this hypothesis, as we observed an upregulation in the expression of *CCL5* in both TUMOR and TME regions. While CCL5 is best known for its role in pro-inflammatory T cell generation and its involvement in HIV pathogenesis, via CCR5 binding[43-46], it also recruits MDSCs and has been implicated in immune suppression in melanoma[47-49]. Elevated MDSC levels prior to initiating immunotherapy in melanoma patients have been associated with poorer treatment response and reduced overall survival, and $CD11b^+$ $HLA\text{-}DR^-$ $CD33^+$ cells have emerged as a predictive biomarker for advanced-stage melanoma prognosis [50]. Collectively, our findings suggest that MDSCs play a central role in shaping the immune landscape of melanoma in PLWH, likely impairing $CD8^+$ T cell responses and contributing to worse clinical outcomes.

Despite inclusion of all confidently identified samples with corresponding clinical data, this study is limited by incomplete information regarding melanoma subtypes and staging, and by the modest sample sizes available for transcriptomic and mIF analyses. Moreover, the absence of an independent validation cohort limits the generalizability of the results and the robustness of the conclusions. These limitations underscore the broader lack of well-annotated biospecimens in this population. Future studies integrating tumor stage, subtype, and demographic data will enable more comprehensive and interpretable analyses. Nonetheless, the significant differences identified here provide a strong rationale for future, more focused biological investigations. These should aim to isolate the immune features of primary versus metastatic tumors in PLWH, further characterize the immature phenotype and functional role of MDSCs in PLWH, and perform functional assays on $CD8^+$ T cells to better understand how their altered states affect anti-tumor

466 responses. Such efforts will be critical to identifying actionable targets within both the T cell and myeloid
467 compartments, ultimately guiding strategies to restore T cell function or limit MDSC accumulation.

468 Our investigation demonstrates that, despite effective ART, HIV infection fundamentally alters
469 melanoma progression, as evidenced by changes in $CD8^+$ T cell subsets and an immunosuppressive
470 myeloid cell presence within the tumors. These immune disruptions, combined with delayed healthcare
471 responses and an increased risk for metastasis, likely contribute to the elevated mortality rate observed in
472 PLWH. Collectively, these findings underscore the urgent need for inclusive clinical trials and targeted
473 therapeutic strategies to address the unique challenges faced by PLWH and improve cancer outcomes for
474 this population.

475

476 **References.**

477 1. Deeks SG, Lewin SR, Havlir DV: The end of AIDS: HIV infection as a chronic disease. Lancet
478 382:1525-33, 2013
479 2. Escota GV, O'Halloran JA, Powderly WG, et al: Understanding mechanisms to promote
480 successful aging in persons living with HIV. Int J Infect Dis 66:56-64, 2018
481 3. Cantero-Perez J, Grau-Exposito J, Serra-Peinado C, et al: Resident memory T cells are a cellular
482 reservoir for HIV in the cervical mucosa. Nat Commun 10:4739, 2019
483 4. Murray AJ, Kwon KJ, Farber DL, et al: The Latent Reservoir for HIV-1: How Immunologic Memory
484 and Clonal Expansion Contribute to HIV-1 Persistence. J Immunol 197:407-17, 2016
485 5. Cohn LB, Silva IT, Oliveira TY, et al: HIV-1 integration landscape during latent and active infection.
486 Cell 160:420-32, 2015
487 6. Eyawo O, Franco-Villalobos C, Hull MW, et al: Changes in mortality rates and causes of death in
488 a population-based cohort of persons living with and without HIV from 1996 to 2012. BMC Infect Dis 17:174,
489 2017
490 7. Yuan T, Hu Y, Zhou X, et al: Incidence and mortality of non-AIDS-defining cancers among people
491 living with HIV: A systematic review and meta-analysis. EClinicalMedicine 52:101613, 2022
492 8. Coghill AE, Han X, Suneja G, et al: Advanced stage at diagnosis and elevated mortality among
493 US patients with cancer infected with HIV in the National Cancer Data Base. Cancer 125:2868-2876, 2019
494 9. Coghill AE, Shiels MS, Suneja G, et al: Elevated Cancer-Specific Mortality Among HIV-Infected
495 Patients in the United States. J Clin Oncol 33:2376-83, 2015
496 10. Love MI, Huber W, Anders S: Moderated estimation of fold change and dispersion for RNA-seq
497 data with DESeq2. Genome Biol 15:550, 2014
498 11. Becht E, Giraldo NA, Lacroix L, et al: Estimating the population abundance of tissue-infiltrating
499 immune and stromal cell populations using gene expression. Genome Biology 17:218, 2016
500 12. Yang ZZ, Kim HJ, Villasboas JC, et al: Expression of LAG-3 defines exhaustion of intratumoral
501 PD-1(+) T cells and correlates with poor outcome in follicular lymphoma. Oncotarget 8:61425-61439, 2017
502 13. Guegan JP, Peyraud F, Dadone-Montaudie B, et al: Analysis of PD1, LAG3, TIGIT, and TIM3
503 expression in human lung adenocarcinoma reveals a 25-gene signature predicting immunotherapy response.
504 Cell Rep Med 5:101831, 2024
505 14. Grosso JF, Goldberg MV, Getnet D, et al: Functionally distinct LAG-3 and PD-1 subsets on
506 activated and chronically stimulated CD8 T cells. J Immunol 182:6659-69, 2009
507 15. Qin A, Cai W, Pan T, et al: Expansion of monocytic myeloid-derived suppressor cells dampens T
508 cell function in HIV-1-seropositive individuals. J Virol 87:1477-90, 2013
509 16. Singh R, Chakraborty M, Gautam A, et al: Residual immune activation in HIV-Infected individuals
510 expands monocytic-myeloid derived suppressor cells. Cell Immunol 362:104304, 2021
511 17. Bronte V, Brandau S, Chen SH, et al: Recommendations for myeloid-derived suppressor cell
512 nomenclature and characterization standards. Nat Commun 7:12150, 2016

18. El Zarif T, Nassar AH, Adib E, et al: Safety and Activity of Immune Checkpoint Inhibitors in People Living With HIV and Cancer: A Real-World Report From the Cancer Therapy Using Checkpoint Inhibitors in People Living With HIV-International (CATCH-IT) Consortium. J Clin Oncol 41:3712-3723, 2023

19. Suneja G, Boyer M, Yehia BR, et al: Cancer Treatment in Patients With HIV Infection and Non-AIDS-Defining Cancers: A Survey of US Oncologists. J Oncol Pract 11:e380-7, 2015

20. Vora KB, Ricciuti B, Awad MM: Exclusion of patients living with HIV from cancer immune checkpoint inhibitor trials. Sci Rep 11:6637, 2021

21. Barger LN, El Naggar OS, Ha B, et al: Melanoma in people living with HIV: Immune landscape dynamics and the role of immuno- and antiviral therapies. Cancer Metastasis Rev 44:9, 2024

22. Saylor D, Dickens AM, Sacktor N, et al: HIV-associated neurocognitive disorder--pathogenesis and prospects for treatment. Nat Rev Neurol 12:234-48, 2016

23. Thompson LJ, Genovese J, Hong Z, et al: HIV-Associated Neurocognitive Disorder: A Look into Cellular and Molecular Pathology. Int J Mol Sci 25, 2024

24. Kluger HM, Chiang V, Mahajan A, et al: Long-Term Survival of Patients With Melanoma With Active Brain Metastases Treated With Pembrolizumab on a Phase II Trial. J Clin Oncol 37:52-60, 2019

25. Robert C, Carlino MS, McNeil C, et al: Seven-Year Follow-Up of the Phase III KEYNOTE-006 Study: Pembrolizumab Versus Ipilimumab in Advanced Melanoma. J Clin Oncol 41:3998-4003, 2023

26. Atkins MB, Lee SJ, Chmielowski B, et al: DREAMseq (Doublet, Randomized Evaluation in Advanced Melanoma Sequencing): A phase III trial—ECOG-ACRIN EA6134. Journal of Clinical Oncology 39:356154-356154, 2021

27. Jiang Y, Li Y, Zhu B: T-cell exhaustion in the tumor microenvironment. Cell Death Dis 6:e1792, 2015

28. Kaunitz GJ, Cottrell TR, Lilo M, et al: Melanoma subtypes demonstrate distinct PD-L1 expression profiles. Lab Invest 97:1063-1071, 2017

29. Gangaev A, Rozeman EA, Rohaan MW, et al: Differential effects of PD-1 and CTLA-4 blockade on the melanoma-reactive CD8 T cell response. Proc Natl Acad Sci U S A 118, 2021

30. Andrews LP, Butler SC, Cui J, et al: LAG-3 and PD-1 synergize on CD8(+) T cells to drive T cell exhaustion and hinder autocrine IFN-gamma-dependent anti-tumor immunity. Cell 187:4355-4372 e22, 2024

31. Tawbi HA, Schadendorf D, Lipson EJ, et al: Relatlimab and Nivolumab versus Nivolumab in Untreated Advanced Melanoma. N Engl J Med 386:24-34, 2022

32. Amaria RN, Postow M, Burton EM, et al: Neoadjuvant relatlimab and nivolumab in resectable melanoma. Nature 611:155-160, 2022

33. Okoye AA, Picker LJ: CD4(+) T-cell depletion in HIV infection: mechanisms of immunological failure. Immunol Rev 254:54-64, 2013

34. Kelley CF, Kitchen CM, Hunt PW, et al: Incomplete peripheral CD4+ cell count restoration in HIV-infected patients receiving long-term antiretroviral treatment. Clin Infect Dis 48:787-94, 2009

35. Sugita M, Brenner MB: An unstable beta 2-microglobulin: major histocompatibility complex class I heavy chain intermediate dissociates from calnexin and then is stabilized by binding peptide. J Exp Med 180:2163-71, 1994

36. Sade-Feldman M, Jiao YJ, Chen JH, et al: Resistance to checkpoint blockade therapy through inactivation of antigen presentation. Nat Commun 8:1136, 2017

37. Hildner K, Edelson BT, Purtha WE, et al: Batf3 deficiency reveals a critical role for CD8alpha+ dendritic cells in cytotoxic T cell immunity. Science 322:1097-100, 2008

38. Gabrilovich DI: Myeloid-Derived Suppressor Cells. Cancer Immunol Res 5:3-8, 2017

39. Wu Y, Yi M, Niu M, et al: Myeloid-derived suppressor cells: an emerging target for anticancer immunotherapy. Mol Cancer 21:184, 2022

40. Wang L, Zhao J, Ren JP, et al: Expansion of myeloid-derived suppressor cells promotes differentiation of regulatory T cells in HIV-1+ individuals. AIDS 30:1521-1531, 2016

41. Jordan KR, Amaria RN, Ramirez O, et al: Myeloid-derived suppressor cells are associated with disease progression and decreased overall survival in advanced-stage melanoma patients. Cancer Immunol Immunother 62:1711-22, 2013

42. Ostrand-Rosenberg S, Fenselau C: Myeloid-Derived Suppressor Cells: Immune-Suppressive Cells That Impair Antitumor Immunity and Are Sculpted by Their Environment. J Immunol 200:422-431, 2018

43. Signoret N, Pelchen-Matthews A, Mack M, et al: Endocytosis and recycling of the HIV coreceptor CCR5. J Cell Biol 151:1281-94, 2000

44. Cocchi F, DeVico AL, Garzino-Demo A, et al: Identification of RANTES, MIP-1 alpha, and MIP-1 beta as the major HIV-suppressive factors produced by CD8+ T cells. Science 270:1811-5, 1995

45. Liu X, Shah A, Gangwani MR, et al: HIV-1 Nef induces CCL5 production in astrocytes through p38-MAPK and PI3K/Akt pathway and utilizes NF-kB, CEBP and AP-1 transcription factors. Sci Rep 4:4450, 2014

46. Zeng Z, Lan T, Wei Y, et al: CCL5/CCR5 axis in human diseases and related treatments. Genes Dis 9:12-27, 2022

47. Zhang Y, Lv D, Kim HJ, et al: A novel role of hematopoietic CCL5 in promoting triple-negative mammary tumor progression by regulating generation of myeloid-derived suppressor cells. Cell Res 23:394-408, 2013

48. Jackson C, Cherry C, Bom S, et al: Distinct myeloid-derived suppressor cell populations in human glioblastoma. Science 387:eabm5214, 2025

49. Schlecker E, Stojanovic A, Eisen C, et al: Tumor-infiltrating monocytic myeloid-derived suppressor cells mediate CCR5-dependent recruitment of regulatory T cells favoring tumor growth. J Immunol 189:5602-11, 2012

50. Sade-Feldman M, Kanterman J, Klieger Y, et al: Clinical Significance of Circulating CD33+CD11b+HLA-DR- Myeloid Cells in Patients with Stage IV Melanoma Treated with Ipilimumab. Clin Cancer Res 22:5661-5672, 2016

Table 1. Demographics of PLWH and PLw/oH with melanoma cohorts for overall survival calculations, before and after balancing cohorts.

	Before balancing cohorts				After balancing cohorts			
	PLWH n (%)	**PLw/oH n (%)**	**p-Value**	**Std. Diff**	**PLWH n (%)**	**PLw/oH n (%)**	**p-Value**	**Std. Diff**
Total n of patients	1087 (100%)	394,437 (100%)			1082 (100%)	1082 (100%)		
Age at Index (years ± SD)	58.60±12.22	62.78±15.57	0.0000	0.3007	58.59±12.25	58.70±13.08	0.8347	0.0090
Sex								
Male	877 (80.7%)	204,376 (51.8%)	0.0000	0.6408	872 (80.6%)	876 (81.0%)	0.8272	0.0094
Female	193 (17.8%)	179,139 (45.4%)	0.0000	0.6235	193 (17.9%)	190 (17.6%)	0.8658	0.0073
Unknown Gender	17 (1.6%)	10,832 (2.8%)	0.0171	0.0815	17 (1.6%)	16 (1.5%)	0.8608	0.0075
Ethnicity								
Hispanic or Latino	45 (4.1%)	5,908 (1.5%)	0.0000	0.1601	44 (4.1%)	55 (5.1%)	0.2578	0.0487
Not Hispanic or Latino	827 (76.1%)	279,817 (70.1%)	0.0002	0.1163	823 (76.1%)	822 (76.0%)	0.9599	0.0022
Unknown Ethnicity	215 (19.8%)	108,622 (27.6%)	0.0000	0.1835	215 (19.9%)	205 (19.0%)	0.5868	0.0234
Race								
White	916 (84.2%)	326,200 (82.7%)	0.1772	0.0418	915 (84.6%)	924 (85.4%)	0.5881	0.0233
Black or African American	78 (7.2%)	4,104 (1.0%)	0.0000	0.3129	74 (6.8%)	72 (6.7%)	0.8639	0.0074
Asian	≤10	3242 (0.8%)	0.7213	0.0105	≤10	≤10	1.0000	0.0000
Native Hawaiian or Other Pacific Islander	≤10	1567 (0.4%)	0.0063	0.0646	≤10	≤10	1.0000	0.0000
American Indian or Alaska Native	≤10	536 (0.1%)	0.0000	0.1083	≤10	0 (0%)	0.0015	0.1383
Unknown Race	70 (6.4%)	48,985 (12.4%)	0.0000	0.2058	70 (6.5%)	65 (6.0%)	0.6567	0.0191
Other Race	17 (1.6%)	9713 (2.5%)	0.0560	0.0640	17 (1.6%)	16 (1.5%)	0.8608	0.0075
Metastatic Sites								
Lymph Node	52 (4.8%)	5,101 (1.3%)	0.0000	0.2044	51 (4.7%)	51 (4.7%)	1.0000	0.0000
Lung	14 (1.3%)	2,169 (0.6%)	0.0010	0.0774	14 (1.3%)	≤10	0.4116	0.0353
Brain / Meningeal	21 (1.9%)	2,116 (0.5%)	0.0000	0.1266	21 (1.9%)	18 (1.7%)	0.6278	0.0208
Liver	≤10	1,909 (0.5%)	0.0389	0.0522	≤10	≤10	1.0000	0.0000
Comorbidities								
Ischemic heart disease	195 (17.9%)	37,038 (9.4%)	0.0000	0.2508	191 (17.7%)	187 (17.3%)	0.8208	0.0135
Chronic viral hepatitis	85 (7.8%)	1,273 (0.3%)	0.0000	0.3864	80 (7.4%)	76 (7.0%)	0.7395	0.0142
Chronic lower respiratory disease	242 (22.3%)	36,569 (9.3%)	0.0000	0.3622	238 (22.0%)	232 (21.4%)	0.7544	0.0135
Chronic kidney disease	116 (10.7%)	19,621 (5.00%)	0.0000	0.2123	114 (10.5%)	120 (11.1%)	0.6779	0.0179
Hypertensive heart disease	33 (3.0%)	7,490 (1.9%)	0.0062	0.0733	31 (2.9%)	28 (2.6%)	0.6921	0.0170
Type 1 Diabetes Mellitus	22(2.0%)	3,984 (1.0%)	0.0009	0.0830	22(2.0%)	19 (1.8%)	0.6362	0.0203

615 **Table 2. Demographics of PLWH and PLw/oH with melanoma cohorts for immunotherapy survival**
616 **calculations, before and after cohort balancing**
617
618

	Before balancing cohorts				After balancing cohorts			
	PLWH n (%)	**PLw/oH n (%)**	**p-Value**	**Std. Diff**	**PLWH n (%)**	**PLw/oH n (%)**	**p-Value**	**Std. Diff**
Total n of patients	95 (100%)	23,827 (100%)			94 (100%)	94 (100%)		
Age at Index (years ± SD)	61.91 ± 11.48	64.27 ± 14.58	0.1141	0.1804	61.15 ± 11.53	63.15 ± 12.65	0.4744	0.1046
Sex								
Male	75 (79.0%)	14,408 (60.5%)	0.0002	0.4105	75 (79.8%)	74 (78.7%)	0.8572	0.0262
Female	18 (19.0%)	8,878 (37.3%)	0.0002	0.4161	17 (18.1%)	17 (18.1%)	1.0000	0.0000
Unknown Gender	≤10	541 (2.3%)	0.0000	0.3422	≤10	≤10	1.0000	0.0000
Ethnicity								
Not Hispanic or Latino	77 (81.1%)	18,440 (77.4%)	0.3944	0.0903	76 (80.9%)	72 (76.0%)	0.4760	0.1041
Hispanic or Latino	≤10	525 (2.2%)	0.0000	0.3460	≤10	≤10	1.000	0.0000
Unknown Ethnicity	15 (15.8%)	4,862 (20.4%)	0.2650	0.1201	15(16.0%)	19 (20.21%)	0.4485	0.1107
Race								
White	84 (88.4%)	21,016 (88.2%)	0.9474	0.0068	83 (88.3%)	83 (88.3%)	1.000	0.0000
Black or African American	≤10	306 (1.3%)	0.0000	0.3998	≤10	≤10	1.0000	0.0000
Asian	≤10	232 (1.0%)	0.0000	0.4193	≤10	≤10	1.0000	0.0000
Native Hawaiian / Pacific Islander	0 (0%)	23 (0.1%)	0.7619	0.0440	0 (0%)	0 (0%)		
American Indian / Alaska Native	0 (0%)	34 (0.1%)	0.7125	0.0534	0 (0%)	0 (0%)		
Other	≤10	583 (2.5%)	0.0000	0.3326	≤10	≤10	1.0000	0.0000
Unknown	≤10	1,633 (6.19%)	0.1577	0.1307	≤10	≤10	1.0000	0.0000
Metastatic Sites								
Lymph Node	45 (47.4%)	8,082 (33.9%)	0.0057	0.2764	44 (46.8%)	44 (46.8%)	1.0000	0.0000
Lung	12 (12.6%)	3,259 (13.7%)	0.7670	0.0309	12 (12.8%)	11(11.7%)	0.8239	0.0325
Brain / Meningeal	13 (13.7%)	2,364 (9.92%)	0.2211	0.1168	13 (13.8%)	12 (12.8%)	0.8299	0.0313
Liver	≤10	1,969 (8.3%)	0.4243	0.0776	≤10	≤10	1.0000	0.0000
Comorbidities								
Ischemic heart disease	25 (26.3%)	4,351 (18.3%)	0.0427	0.1945	25 (26.6%)	23 (24.5%)	0.7380	0.0489
Chronic viral hepatitis	≤10	144 (0.6%)	0.0000	0.4433	≤10	≤10	1.0000	0.0000
Chronic lower respiratory disease	24 (25.3%)	3,898 (16.4%)	0.0193	0.2207	23 (24.5%)	28 (29.8%)	0.4121	0.1198
Chronic kidney disease	18 (18.9%)	2,069 (8.7%)	0.0001	0.3008	17 (18.1%)	18 (19.2%)	0.8514	0.0273
Hypertensive heart disease	≤10	978 (4.1%)	0.0017	0.2485	≤10	≤10	1.0000	0.0000
Type 1 Diabetes Mellitus	≤10	343 (1.4%)	0.0000	0.3903	≤10	≤10	1.0000	0.0000

619
620
621
622

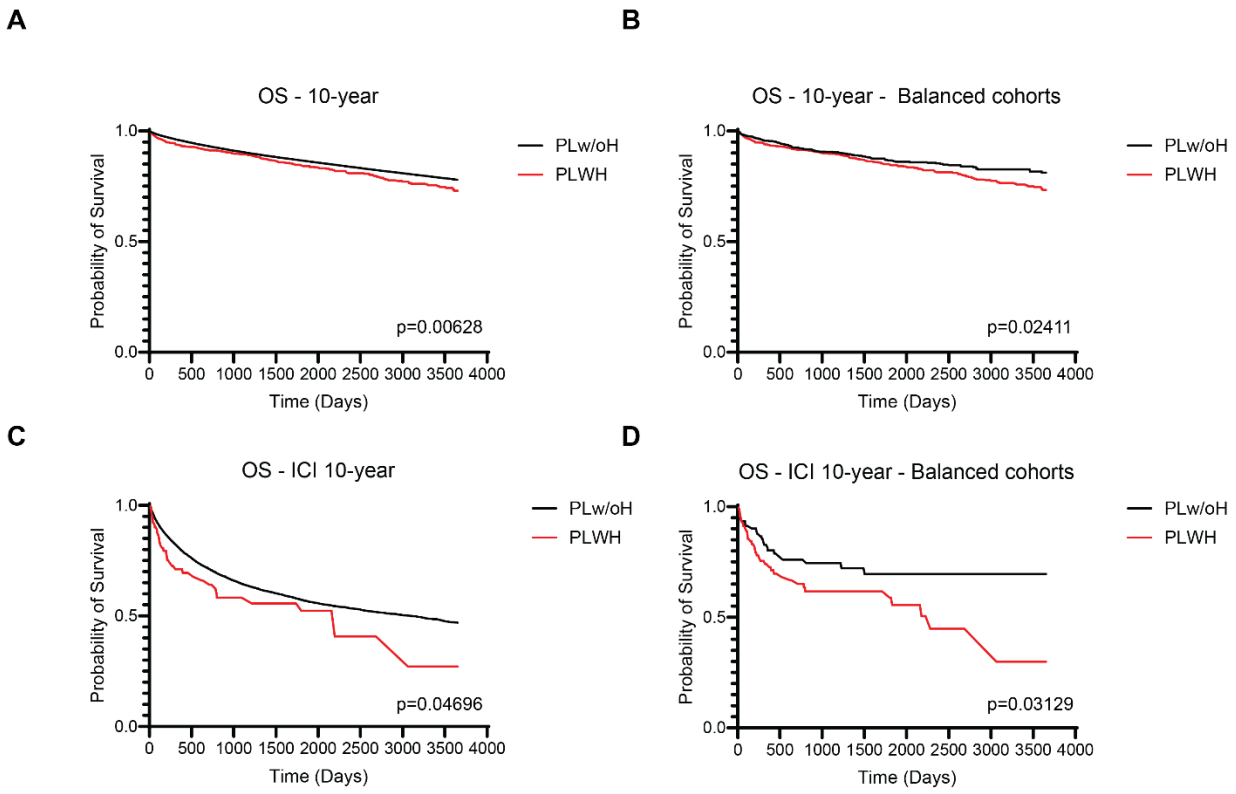

Figure 1. Overall survival rates and immune checkpoint therapy survival rates of PLWH and PLw/oH with melanoma. A-B) Kaplan-Meier graphs representing 10-year survival probability of PLWH and PLw/oH with melanoma. The index event is a melanoma diagnosis. A) Overall survival (OS), including all patients in the cohorts. B) OS after balancing for demographic covariates. C-D) Kaplan-Meier graphs representing 10-year survival probability of PLWH and PLw/oH with melanoma who underwent immune checkpoint therapy. The index event is the treatment start. C) OS including all patients in the cohorts. D) OS after balancing for demographic and clinical covariates. Reported p-values are from a Log-rank sum test between the two cohorts ($p<0.05$ is considered statistically significant).

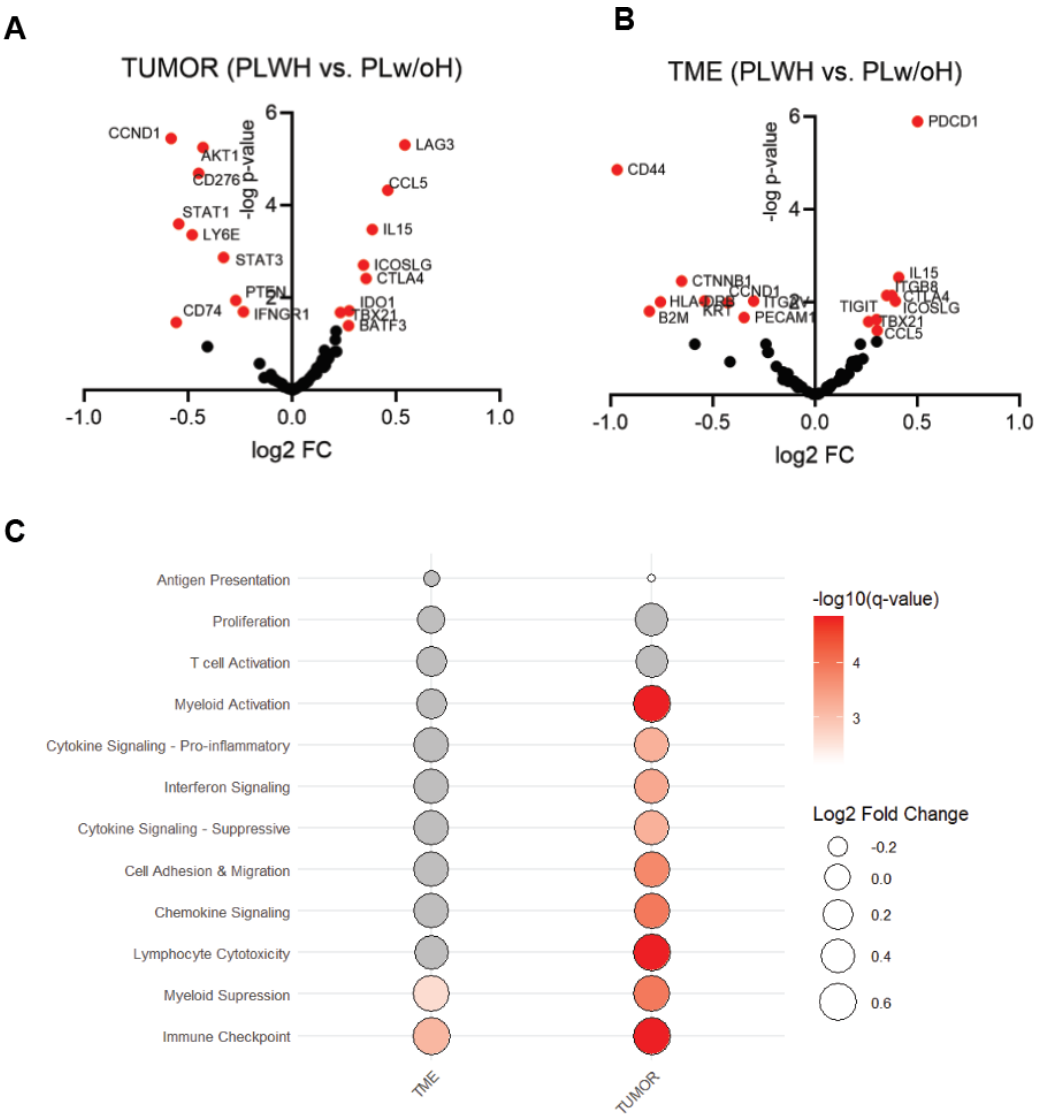

Figure 2. Spatial immune transcriptomic profiling of melanoma samples from PLWH and PLw/oH. Volcano plots for A) TME and B) TUMOR, comparing immune gene expression of PLWH vs PLw/oH melanoma samples (n=11); log2 fold change is on the x-axis, and -log10 of adjusted p-value is on the y-axis. Values were calculated by the DEseq2 algorithm (data points in red have an adjusted p-value <0.05). C) Bubble plot representation of immune signaling gene set analysis performed by running the MCPcounter algorithm on the gene expression matrix. Bubble plot size represents the log2 fold change of MCPcounter scores (PLWH vs. PLw/oH), and bubble color represents the adjusted p-value (q-value in a multiple Welch t-test with FDR of 0.01) for the TUMOR and TME areas (PLWH vs. PLw/oH). A q-value<0.01 was considered significant; comparisons with non-significant q-values are represented in grey.

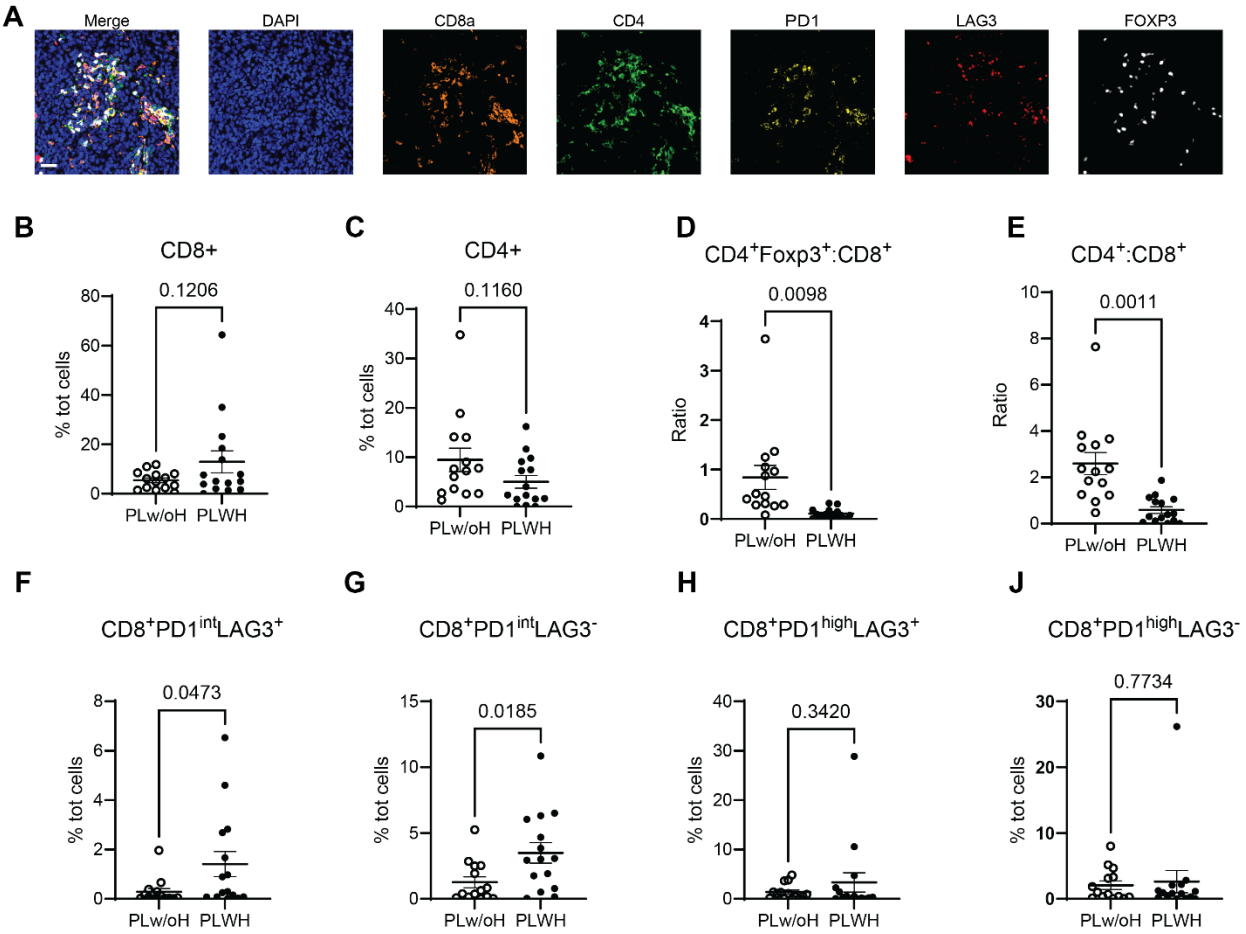

Figure 3. Multiplex IF assessment of T-cell populations' abundance and immune checkpoint expression in melanoma samples from PLWH and PLw/oH. A) Representative images depicting each staining marker of our T cell multiplex immunofluorescence (mIF) panel, which was used to analyze melanoma tumors from PLWH and PLw/oH. The scale bar represents 50 µm. Quantification of mIF was performed on PLWH (n=15) and PLw/oH (n=14) tumor samples. Percentage of B) $CD8^+$ and C) $CD4^+$ T cells over the total number of cells. D) Ratio of $CD4^+Foxp3^+$ to $CD8^+$ T cells, and E) $CD4^+$ T cells to $CD8^+$ T cells. Percentage of $PD1^{int}$ $CD8^+$ T cells that are F) $LAG3^+$ and G)$LAG3^-$ over the total number of cells. Percentage of $PD1^{HIGH}$ $CD8^+$ T-cells that are H) $LAG3^+$ and J) $LAG3^-$ over the total number of cells. The represented p-values are from a Welch's t-test; $p < 0.05$ is considered significant, and error bars represent SEM.

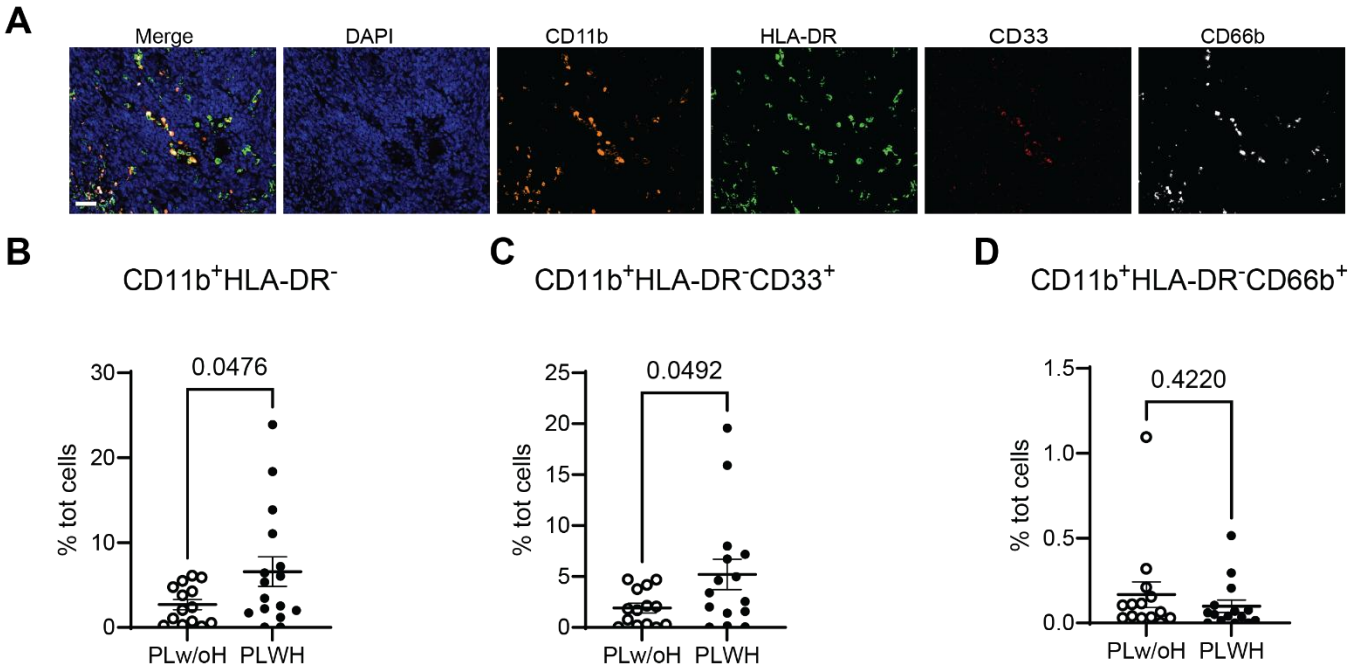

Figure 4. Multiplex IF assessment of myeloid populations' abundance in melanoma samples from PLWH and PLw/oH. A) Representative images depicting each staining marker used in our myeloid multiplex immunofluorescence (mIF) panel, used to analyze melanoma tumor samples from PLWH and PLw/oH. The scale bar represents 50 µm. Quantification of mIF was performed on PLWH (n=15) and PLw/oH (n=14) tumor samples. Percentage of B) $CD11b^{+}HLA\text{-}DR^{-}$, C) $CD11b^{+}HLA\text{-}DR^{-}$, $CD33^{+}$, D) $CD11b^{+}HLA\text{-}DR^{-}$, $CD66b^{+}$, over the total number of cells. The represented p-values are from a Welch's t-test; $p < 0.05$ is considered significant, and error bars represent SEM.